Coherent Structure Tracking (CST)

Th. Roudier, IRAP Toulouse
M. Chane-Yook, IAS Orsay

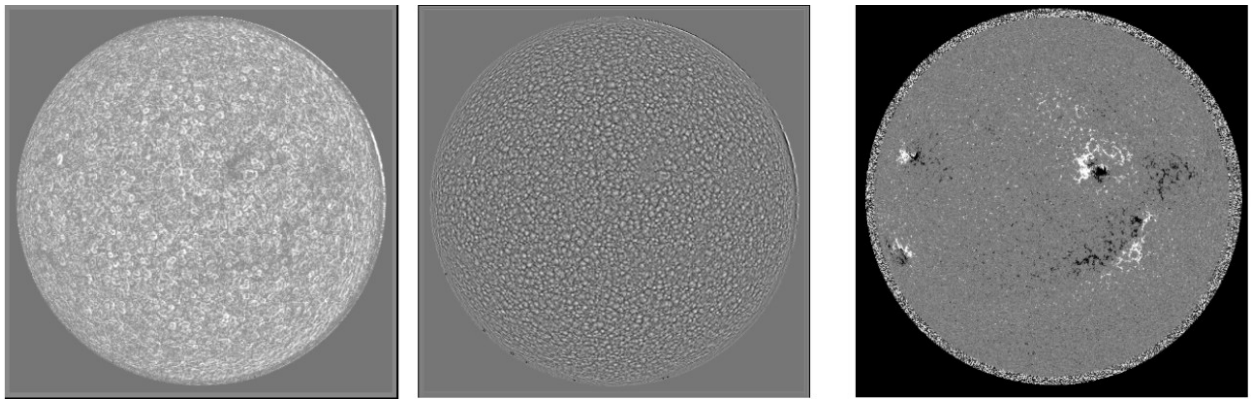

SCHEDULE

- Different methods to determine horizontal flow fields

- First steps of the CST for ground data small fields

- CST for Full Sun SDO data

- reduction CST 3 steps : corrections , velocity (Vx,Vy), transformations

- Some examples of results with and without solar rotation

Different methods to determine horizontal flow fields

The determination of granule motions is not a simple matter and in 1980-1990, only *three techniques* have been developed by different groups:

Local Correlation Tracking (LCT)
by Shine and November Simon 1986 -1989

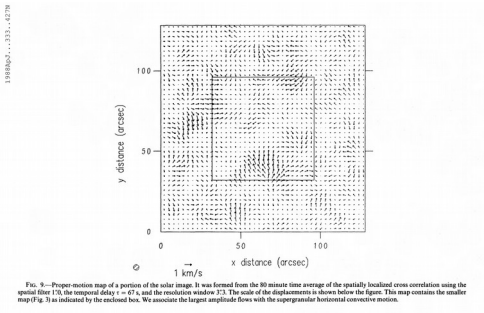

Feature Tracking (FT) by Strous (1994, 1995a).

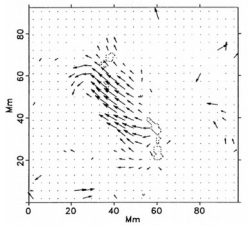

Figure 5: Flow field of flux elements of leading polarity in a young active region, derived with the simple identification strategy. The dotted contours indicate the positions of sunspots and pores.

Time-distance helioseismology by Duvall 1996

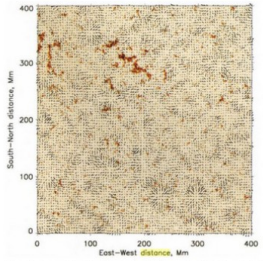

Figure 8. A comparison between the absolute value of magnetic field (in color) and the simulated surface velocity from the time-distance pictures (arrows). The longest arrow is for 1 km s^{-1} velocity.

Local correlation tracking (LCT, 1988)

Promoted November & Simon

The method is based on a simple but powerful idea :

Mathematically this idea is expressed in terms of **a correlation function between two instants.**

Calculating the rigid translation of small image elements (window, subimage) between two consecutive frames (images)

The motion is calculated by the shift that gives the highest correlation between the corresponding subimages

*The selection of the sub-areas is performed by means of a window which is usually set to be a **Gaussian function with a Full-Width at Half** (FWHM). **Maximum (FWHM)** adapted to the desired size for the correlation patch and depending on the **spatial-scale** of the structures we are about to track.*

Advantage of LCT: simple and fast method

Disavantage of LCT:
- low spatial resolution
- under-estimate amplitude of the velocity
- Takes granule and intergranule (in the spatial window) difficulty to separate average velocity vectors can be derived for each class of entities present in the image (for instance for faculae of either magnetic polarity).
- Full Sun crunch<==========

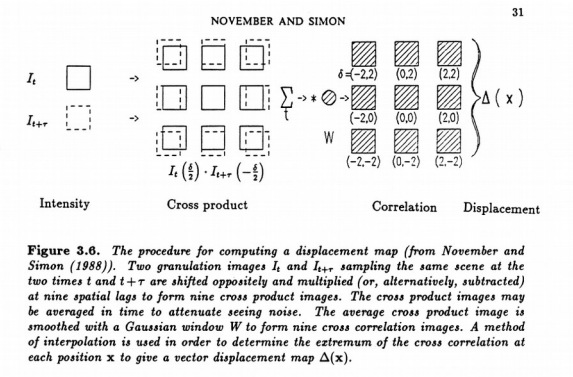

Figure 3.6. *The procedure for computing a displacement map (from November and Simon (1988)). Two granulation images I_t and $I_{t+\tau}$ sampling the same scene at the two times t and $t+\tau$ are shifted oppositely and multiplied (or, alternatively, subtracted) at nine spatial lags to form nine cross product images. The cross product images may be averaged in time to attenuate seeing noise. The average cross product image is smoothed with a Gaussian window W to form nine cross correlation images. A method of interpolation is used in order to determine the extremum of the cross correlation at each position* $\mathbf{x}$ *to give a vector displacement map* $\Delta(\mathbf{x})$.

Features Tracking (1994, 1995)

promoted by Strous

Feature Tracking (FT) is another algorithm first applied to solar data by Strous.
The idea is to assume granules are **objects advected by an underlying flow** which we wish to measure.

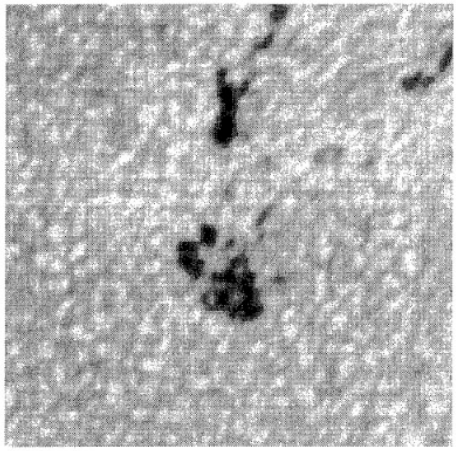

Figure 1: A continuum image of a young active region, observed at the Swedish Vacuum Solar Telescope in La Palma, Spain, showing granulation and sunspots.

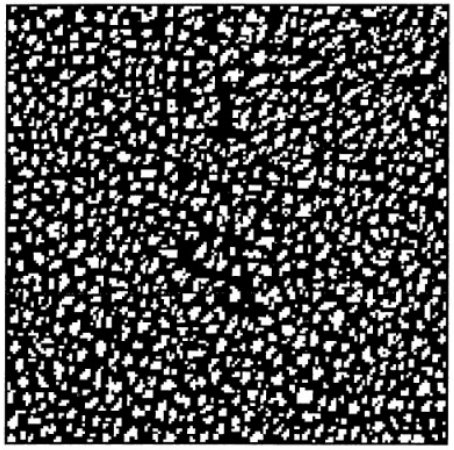

Figure 2: The segmented image corresponding to Fig. 1 (seeking bright objects).

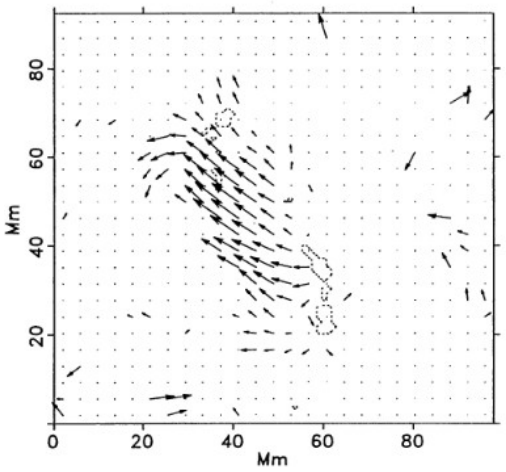

Figure 5: Flow field of flux elements of leading polarity in a young active region, derived with the simple identification strategy. The dotted contours indicate the positions of sunspots and pores.

Nota : However, the comparison of the results of these two techniques, **LCT and FT**, applied to the same set of data (Simon et al. 1995, Strous1995b), shows **discrepancies in the resulting velocity, divergence and vorticity fields (derivative)** .

Time-distance helioseismology (1996)

promoted by Duvall

This method uses the measurement of the difference in speed of acoustic waves propagating in opposite directions to work ous the velocity of the fluid.

Tomographic inversion method has been used to reconstruct the **3D maps of flows** 0.6 arcsec/pixel (SOHO). **.**

*By **crosscorrelating the signal at one location** with that on annuli centered on the location, it is possible to measure times for waves to travel over known subsurface ray paths. With some variations on this theme, it is possible **to measure horizontal and vertical flows***

Nota : low spatial and temporal resolution

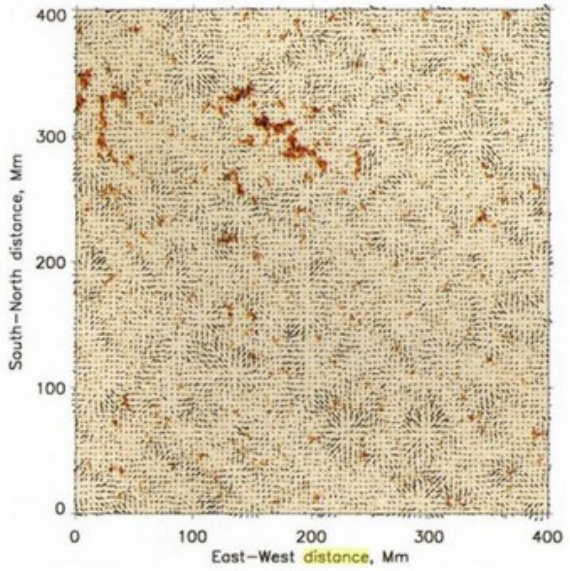

Figure 8. A comparison between the absolute value of magnetic field (in color) and the simulated surface velocity from the time-distance pictures (arrows). The longest arrow is for 1 km s^{-1} velocity.

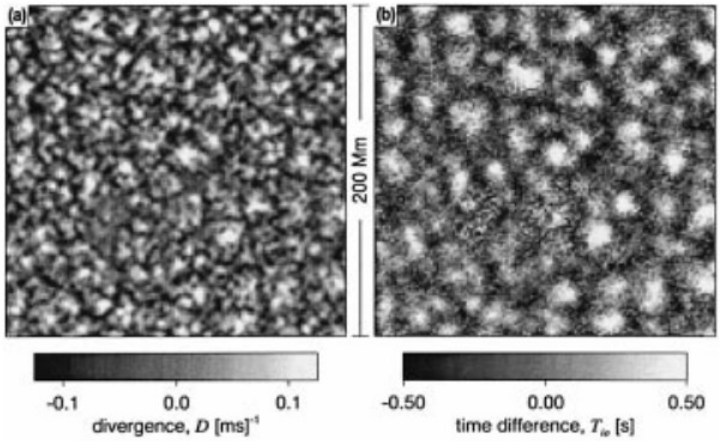

Figure 1. (a) A 512-min average image of divergence D calculated from correlation tracking measurements of the near-surface velocity field for one of the blocks (block 2 of Table I). (b) A 512-minute average image of travel-time differences T_{io} measured using time-distance helioseismology for the same block. An active region coincides with the textured region just below frame center.

Different methods to determine horizontal flow fields

In 2000, other techniques have been developed by different groups:

Balltracking method (Potts 2004)

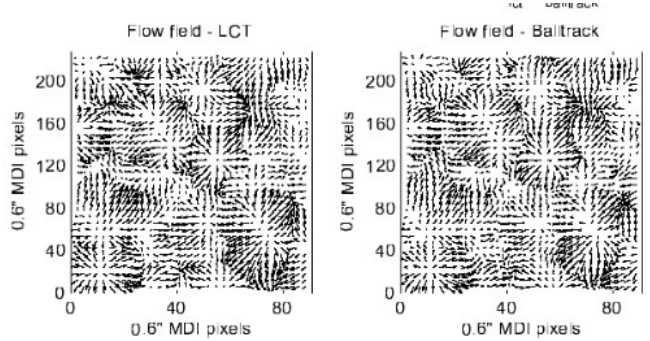

Fig. 8. Comparison of Balltrack and LCT recovered velocity fields from real MDI data. The original data set consisted of 240 256 × 256 pixel (approx. 150 × 150″) frames taken at one minute intervals.

DAVE (Chae 2008)

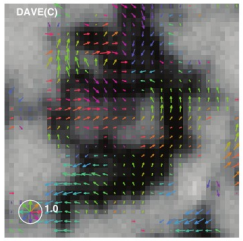

DeepVel (Asensio RAMOS, 2017)

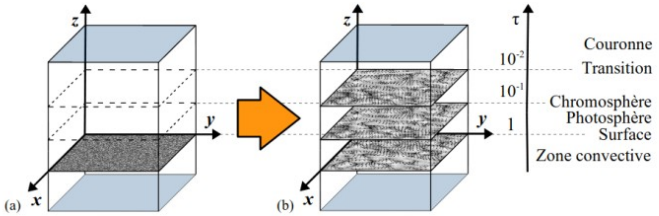

Balltracking method (Potts 2004)

The **motion of the balls** is calculated entirely in **velocity space (written in Matlab).**

The **balls have mass and momentum** ====> the granulation cells pushing a ball.

The **momentum of the ball** **"predict" where to go at the next time step** (method efficient).

To track photospheric flows ⇒ thousands of these trackers are released to get the surface motions.

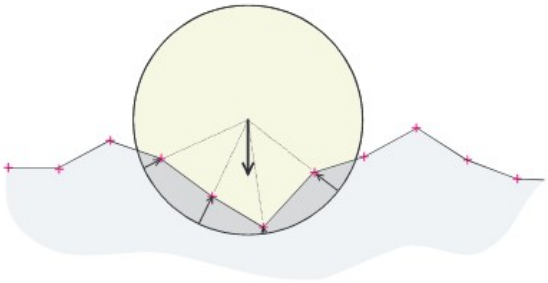

Fig. 3. Cross section of a ball on a granulation surface. The ball penetrates the surface, with the force on the ball from each surface point proportional to the penetration distance.

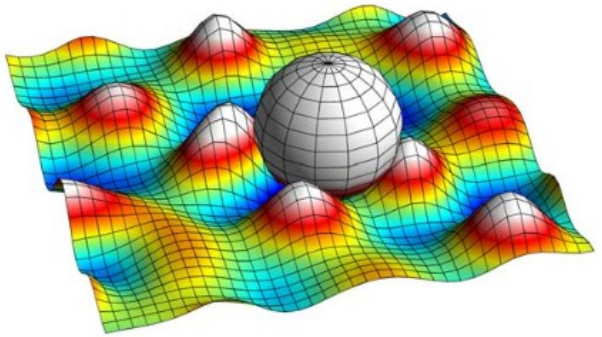

Fig. 1. One of the tracers or balls, floating on a simulated granulation surface. As the peaks that represent the granulation cells move and evolve, they push the ball around.

Advantage : tracking accuracy, more efficient than LCT

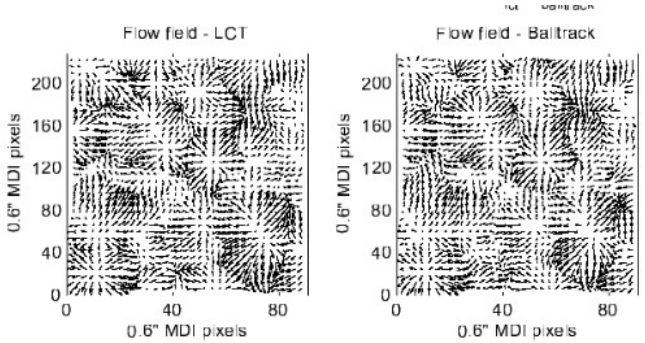

Fig. 8. Comparison of Balltrack and LCT recovered velocity fields from real MDI data. The original data set consisted of 240 256 × 256 pixel (approx. 150 × 150″) frames taken at one minute intervals.

DAVE (Chae 2008)

Differential affine velocity estimator (DAVE).

(NAVE) new technique called the nonlinear affine velocity estimator.

To be applied on magnetogram

This technique implements a variational principle to minimize deviations in the magnitude of the magnetic induction equation constrained by an affine velocity profile, which depends linearly on coordinates, within a windowed subregion of the magnetogram sequence

The algorithm imposes a global criterion to have the **velocity vector vary smoothly.**

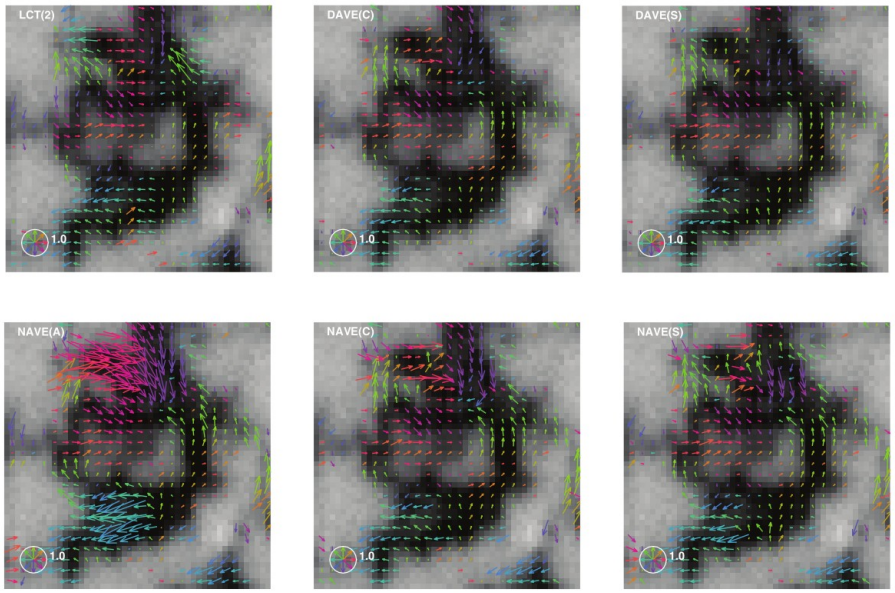

FIG. 11.—Velocity fields obtained from real magnetograms using different methods. The colors of the arrows represent the directions as indicated inside the circle.

DeepVel (Asensio RAMOS, 2017)

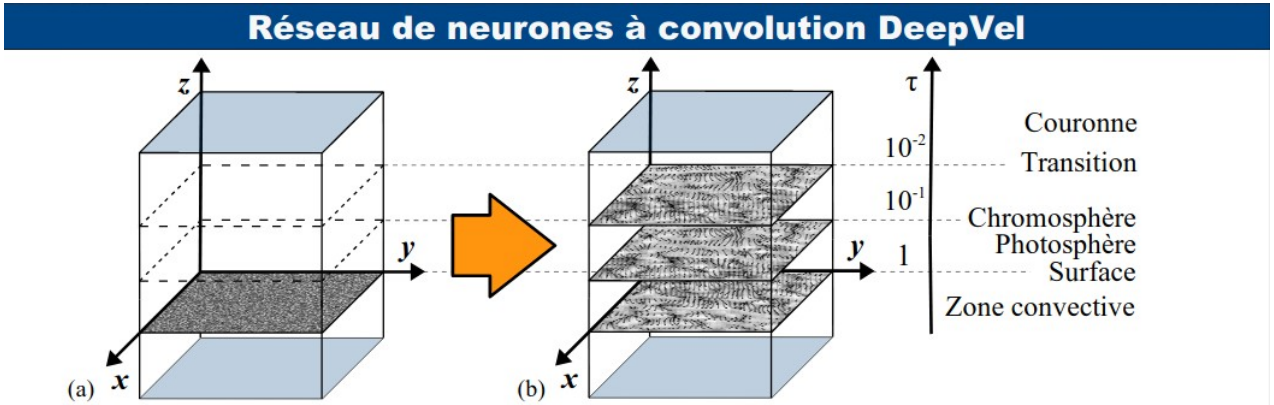

Figure 2: Réseau DeepVel (Asensio Ramos *et al.*, 2017). (a) **Données d'entrée:** Intensité du continu à la surface du Soleil (profondeur optique $\tau \sim 1$). (b) **Sorties du réseau:** Composante horizontale de la vitesse aux profondeurs optiques $\tau=1$, 10^{-1} et 10^{-2}. L'ensemble d'entraînement inclut 2000 exemples de 50×50 pixels extraits de la simulation de Stein & Nordlund (2012) et échantillonnés à la résolution spatiale de l'instrument SDO/HMI (Figure 3(b)).

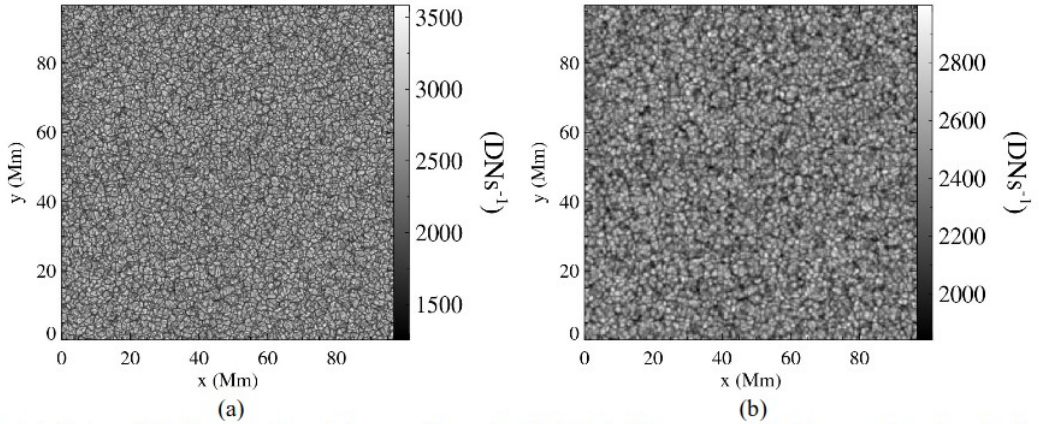

Figure 3: (a) Intensité du continu à la surface du Soleil telle que calculée par la simulation de Stein & Nordlund (2012) avec une résolution spatiale de 96 km par pixel. (b) Même image, échantillonnée à la résolution spatiale de l'instrument SDO/HMI (368 km par pixel).

DeepVel (Asensio RAMOS, 2017)

Résultats – Données synthétiques

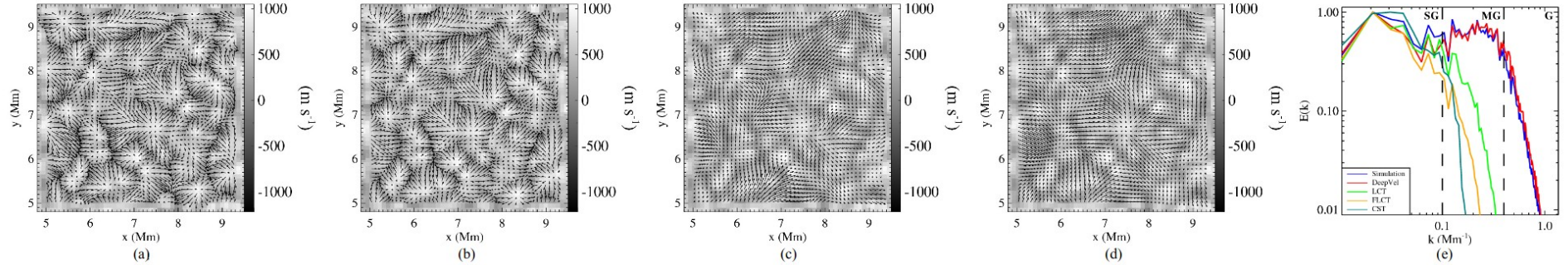

Figure 4: Champs de vecteurs de la vitesse horizontale du plasma tels que calculés par (a) la simulation de Stein & Nordlund (2012) échantillonnée à la résolution spatiale de l'instrument SDO/HMI (**champ de référence**), (b) le réseau de neurones **DeepVel** entraîné avec les résultats de la simulation de Stein & Nordlund (2012), (c) ***Local Correlation Tracking*** (LCT: November & Simon (1988)) et (d) ***Fourier-based Local Correlation Tracking*** (FLCT: Fisher & Welsch (2008)). La composante verticale de la vitesse calculée par la simulation de Stein & Nordlund (2012) est affichée en arrière-plan. À l'intérieur des granules, le plasma monte (vitesse verticale positive) et les vecteurs de la vitesse horizontale **divergent**. À l'interstice entre les granules, le plasma coule vers l'intérieur de l'étoile (vitesse verticale négative) et les vecteurs de la vitesse horizontale **convergent**. (e) Le **spectre de l'énergie cinétique** E(k) en fonction du nombre d'onde k (qui est inversement proportionnel à l'échelle spatiale, à un facteur 2π près) montre qu'il y a un bon accord entre le champ de référence et les vitesses inférées par DeepVel aux échelles supergranulaire (SG: 10 Mm et plus), mesogranulaire (MG: entre 1 Mm et 10 Mm) et granulaire (G: 1 Mm ou moins).

Résultats – Données SDO/HMI

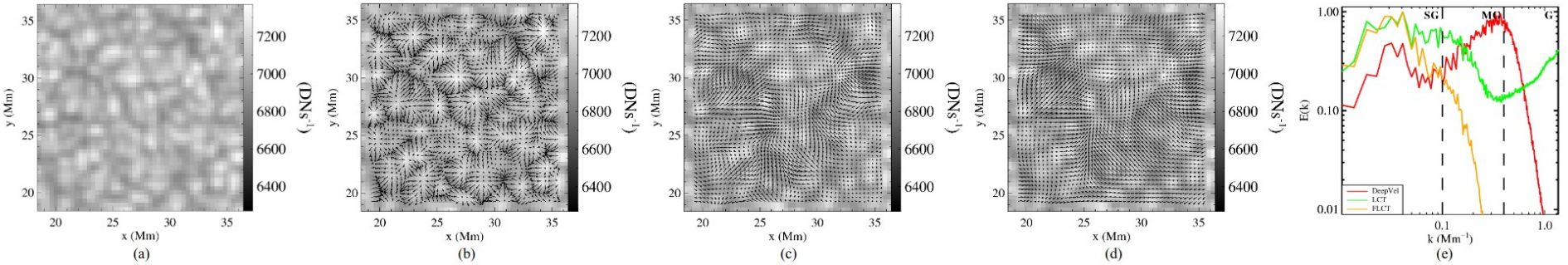

Figure 5: (a) **Intensité du continu mesurée par l'instrument SDO/HMI** le 2010-10-08. (b) **Champs de vecteurs de la vitesse horizontale du plasma** tels que calculés par (b) le réseau de neurones **DeepVel** entraîné avec les résultats de la simulation de Stein & Nordlund (2012), (c) **LCT** et (d) **FLCT**. L'intensité du continu mesurée par l'instrument SDO/HMI est affichée en arrière-plan. À l'intérieur des granules, le plasma ascendant est plus chaud (intensité plus élevée) et les vecteurs de la vitesse horizontale **divergent**. À l'interstice entre les granules, le plasma descendant refroidit (intensité plus faible) et les vecteurs de la vitesse horizontale **convergent**. (e) Le **spectre de l'énergie cinétique** E(k) en fonction du nombre d'onde k (qui est inversement proportionnel à l'échelle spatiale, à un facteur 2π près) montre que seul DeepVel reproduit les variations attendues aux échelles mesogranulaire (MG: entre 1 Mm et 10 Mm) et granulaire (G: 1 Mm ou moins).

Conclusion

- **Comparaison: Les champs de vitesse générés par le réseau de neurones DeepVel capturent les propriétés de la granulation solaire à des échelles spatiales et temporelles qui sont compatibles avec celles des observations effectuées par l'instrument SDO/HMI.**
- **Futur: Incorporation des vitesses à titre d'observations synthétiques dans un modèle magnétohydrodynamique des couches du Soleil pour effectuer l'assimilation des données.**

CST (Roudier 1999)
Ground solar observations

Small fields

The Coherent Structure Tracking (CST) algorithm is **an improved version** of the one already used by Strous :

- before determining the zero-curvature contour which defines the granule we **first filter the image** with a gaussian window which has the effect of removing some noise;

- we make the **segmentation**; through opening operations, we further break narrow isthmuses and **remove thin protusions**; finally, we eliminate all granules which deform too much.

-The **motion of granules is pinpointed by that of the barycenter** of the surface enclosed by the contour, while Strous (1994) tracks the intensity maximum enclosed by the contour. Our tracking is more robust, as it is not sensitive to intensity fluctuations inside granules and represents more faithfully the mean displacement of these coherent structures.

Principe of the CST

- assume granules are objects advected by an underlying flow which we wish to measure.
- the lifetime of a coherent object (granules) is defined between its appearance and disappearance if the granule.
- if granule split : the life is stopped and children=new granules
- if granule merge : the lives of granule that merge are stopped and the new granule issued from merging = new granule

WE CAN FOLLOW COHERENT STRUCTURES BETWEEN THEIR BIRTH AND DEATH

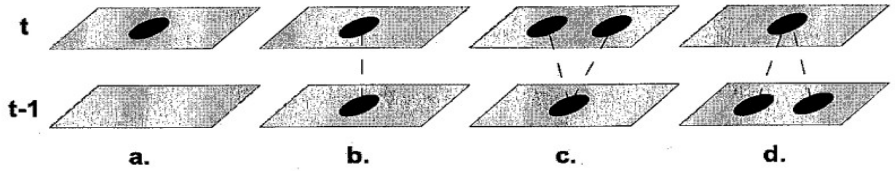

Fig. 1: CST principle

During their lifetime, granules can split or merge into multiple objects. Disappearance or appearance between two successive frames must be taken into account. Then, the life of coherent objects (i.e granules) is defined between its appearance and disappearance if the granule does not split or merge. When the granule splits (Fig. 1.c), the life of granule is stopped and its "children" are considered as new granules. In the same way, when granules merge (Fig. 1.d), the lives of the granules that merge are stopped and the new granule issued from the merging is considered as a new granule. Thus, we can follow a coherent structure between their birth and death.

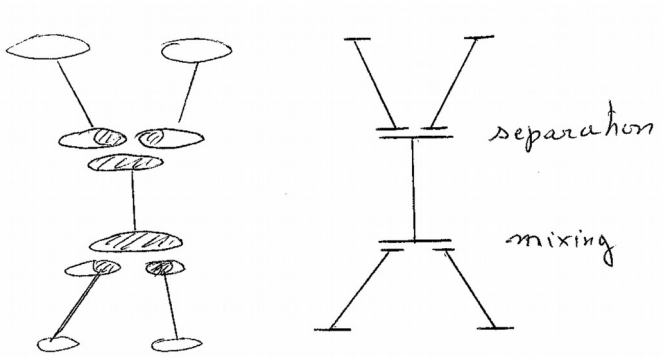

CST (Roudier 1999)
Ground solar observations

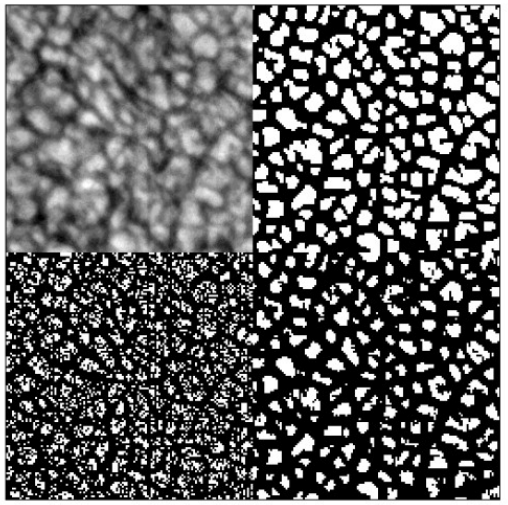

1000 km

2000 km

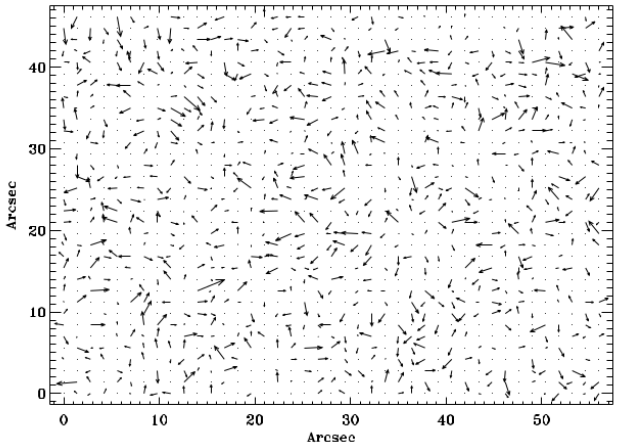

Fig. 7. Velocity field determined by CST with a temporal window of 10 mn.

Temporal window 10 minutes
Spatial window 1000 km

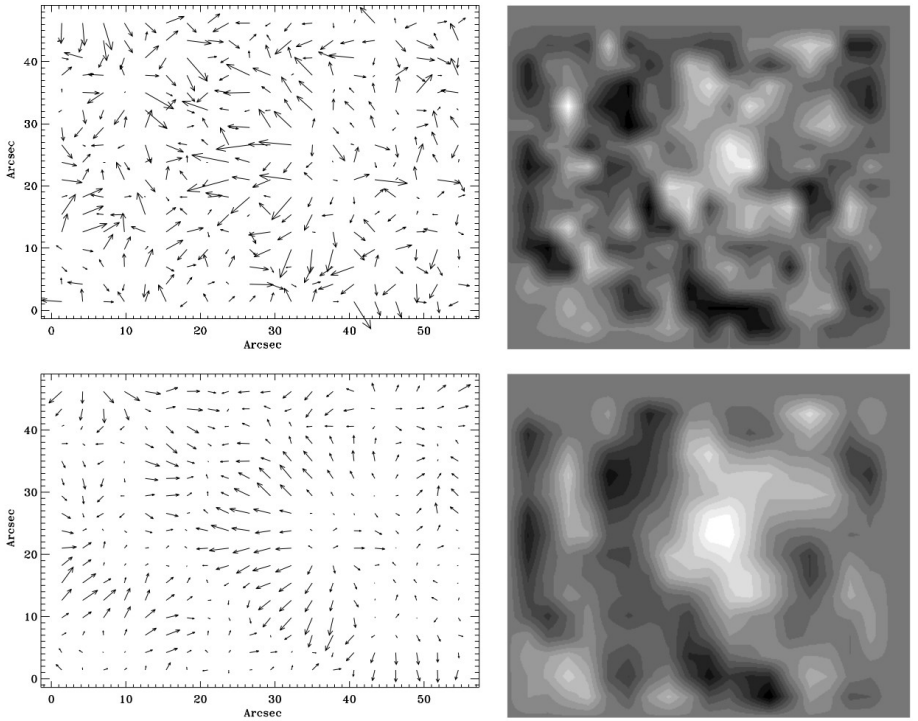

Fig. 13. Velocity field (left) and divergence field (right) obtained using the CST algorithm (top) or LCT algorithm (bottom). Data are time-averaged over 30 mn. One question raised by such plots is, how confident can we be in the reality of the structures shown in these figures?

Temporal window 30 minutes
Spatial window 2000 km

CST
Wavelet multi-resolution representation

Granules do not sample the field of view uniformly, and **reconstruction of the velocity field**, along with its derivatives like divergence or curl, requires some interpolation.

There are many ways of performing such an operation; however, classical methods, like polynomial interpolation,would propagate errors and noise everywhere.

We thus selected a **method based on wavelet multi-resolution representation (MRA) which projects data onto Daubechies wavelets**.

The spatial window needs to be larger than 2.5 Mm Rieutord (2001)

- raw: b (brut) raw ux and uy from CST (586 x 586 pixels)
- high: h: first high resolution wavelet filter (Daubechies)
- middle: m second wavelet filtering (Daubechies) half resolution of "h"
- large: l third filtering by wavelet (Daubechies) resolution half of "m"
- extra-large: k fourth filtering by wavelet (Daubechies) resolution half "l"

SDO data the resolution will be (if we takebin_sp = 7 (pixels) file speeds (ux, uy) on a size of 586x586 pixels
h = 2.5 Megameters (Mm)
m = 5.0 Mm
l = 10 Mm
k = 20 Mm

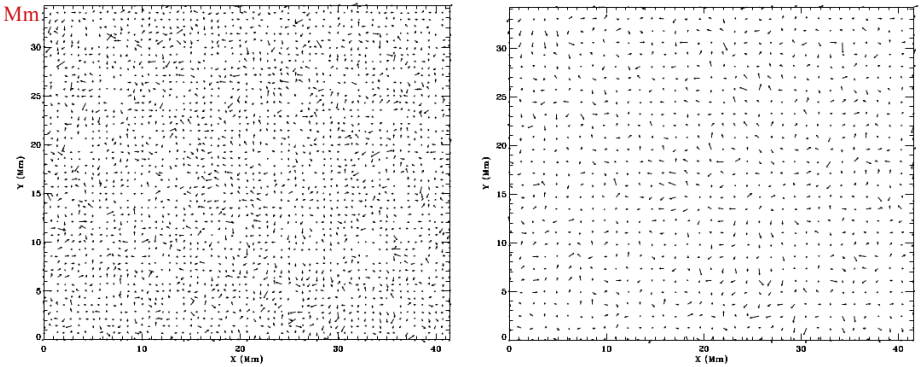

Fig. 6. To the *left*, the velocity field with a small mesh size (713 km) is complete with 83% of data, while on the *right*, using a larger mesh size of 1223 km, the velocity field is complete to 99%. Patterns of velocities are easily identified between the two. We used a time interval of 15 min.

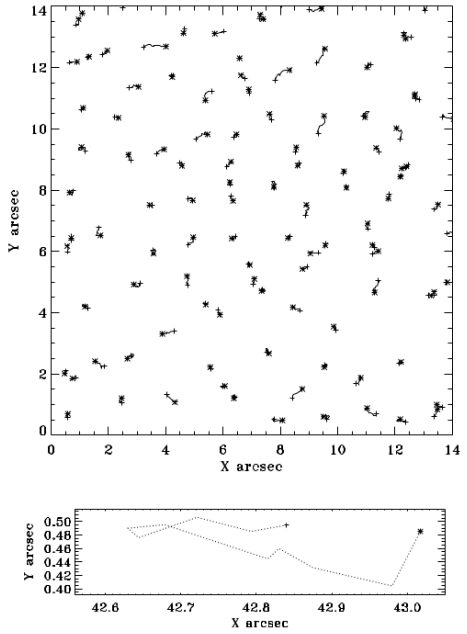

Fig. 3. Trajectories of granules in a five-minute time sequence. *Top*: Granule displacements in a small subfield. *Bottom*: enlarged view of a granule trajectory. Data are from the 1988 Pic-du-Midi series (e.g. Muller et al. 1992).

CST (Roudier 2012)

Full Sun HMI/SDO data

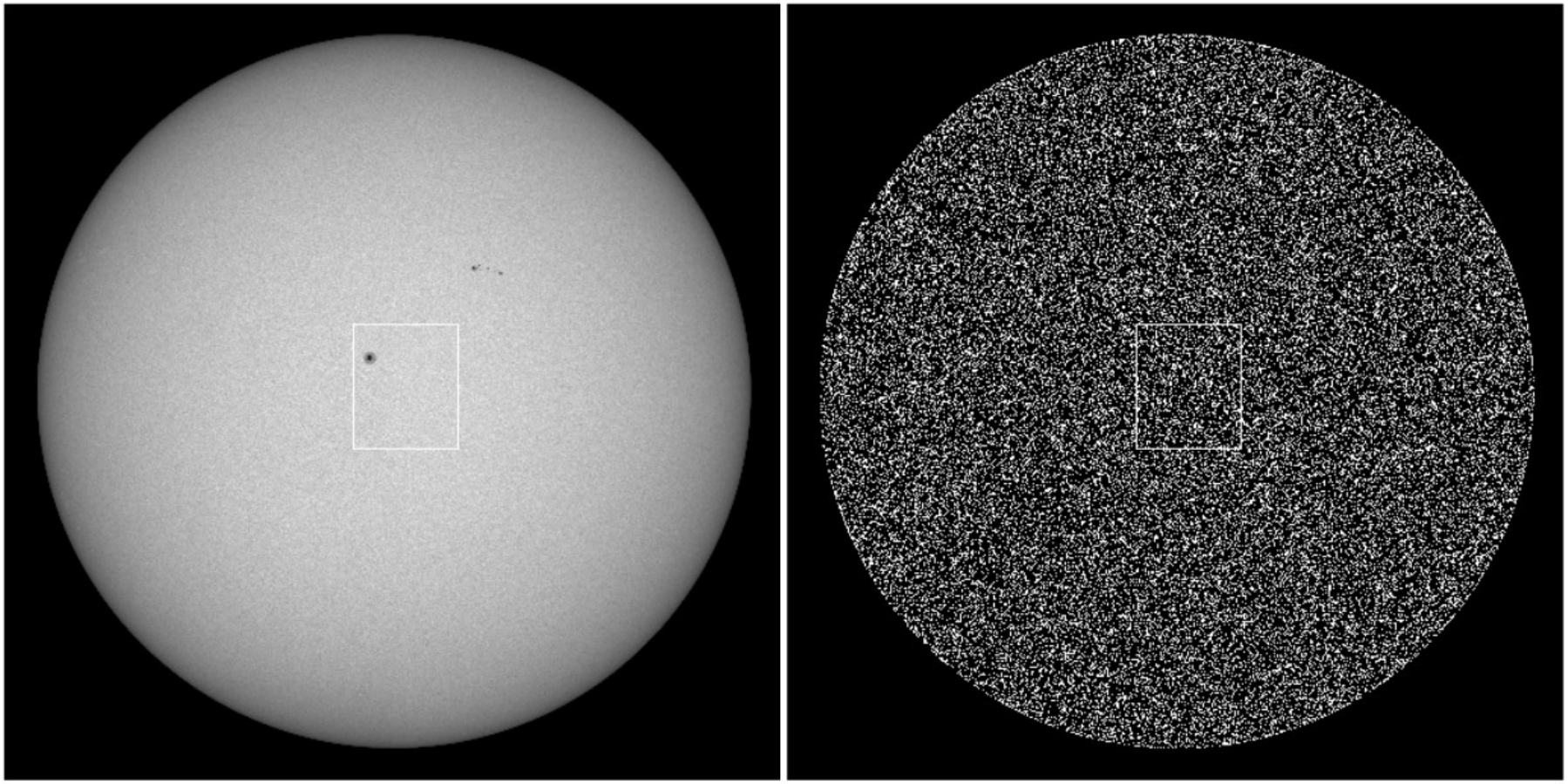

Fig. 1. Full Sun HMI/SDO white-light on August 30, 2010 (*left*) and the segmented map, in which about 500 000 granules are detected (*right*).

CST on SDO data : superposition of granule area at t and t+1

CST (Roudier 2012)
Full Sun

The length scale (spatial window) needs to be larger than 2.5 Mm =7pixel for SDO data

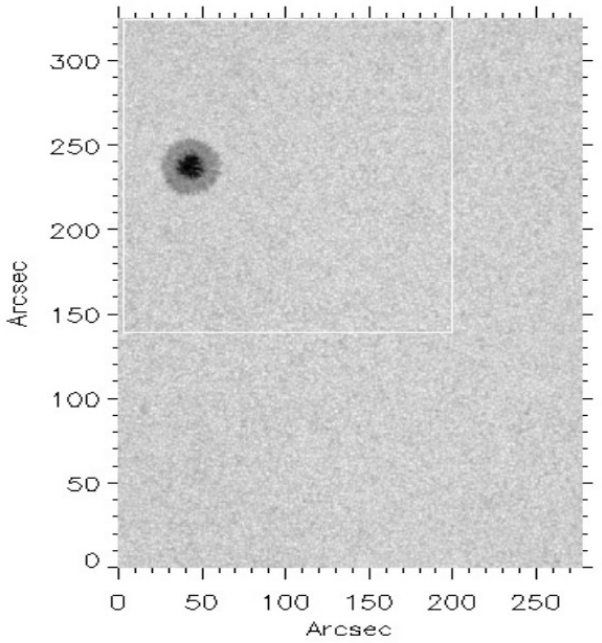

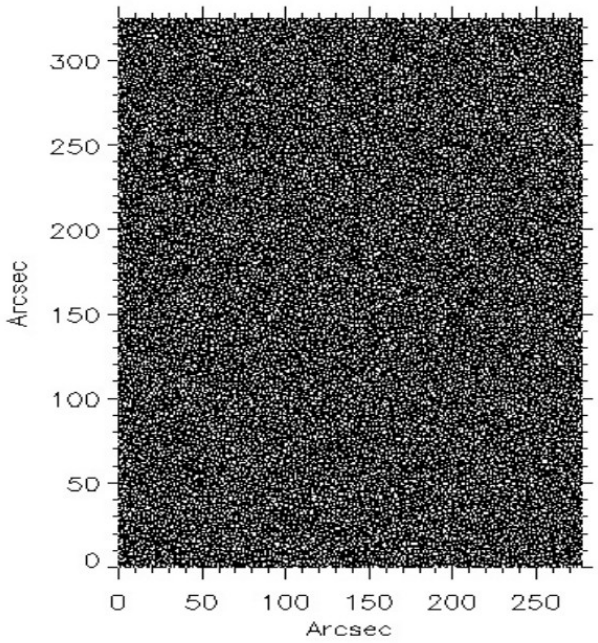

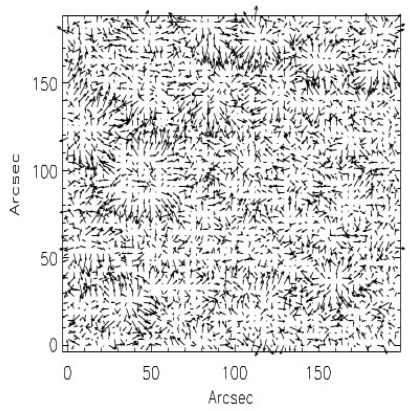

30 min
2.5 Mm

CST (Roudier 2012)
Full Sun

Solar rotation removed, spatial window=2.5 Mm, temporal window=2h

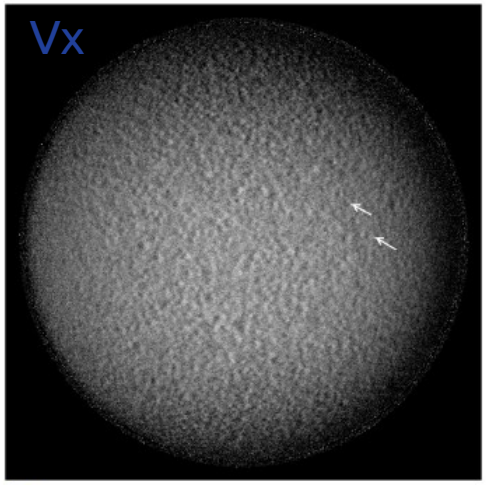

Fig. 3. Full Sun V_x component from a two-hour sequence, spatial resolution 2.5 Mm. Arrows indicate the location of supergranule visible also on the Doppler map.

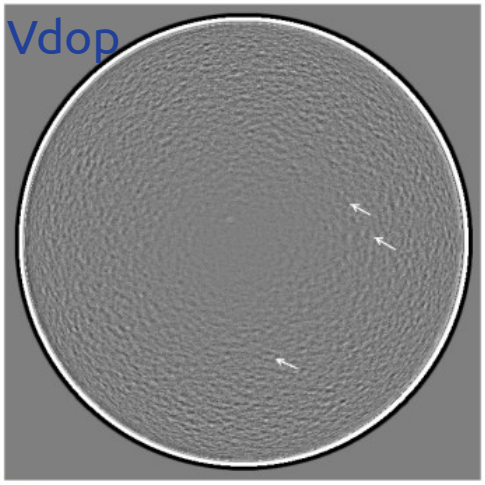

Fig. 5. Averaged Dopplergram from two-hour sequence where the solar rotation has been removed. Arrows indicate the location of supergranule.

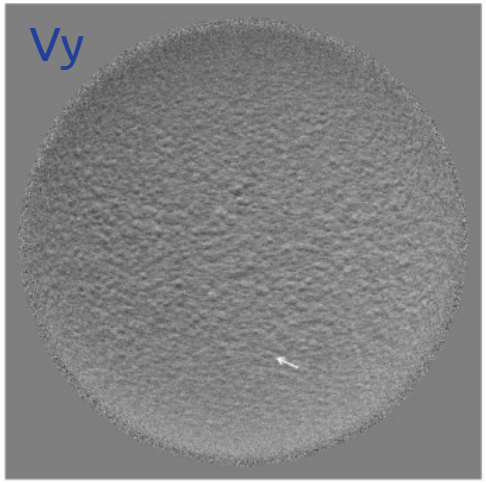

Fig. 4. Full Sun V_y component from two-hour sequence, spatial resolution 2.5 Mm. Arrow indicates the location a supergranule visible also on the Doppler map.

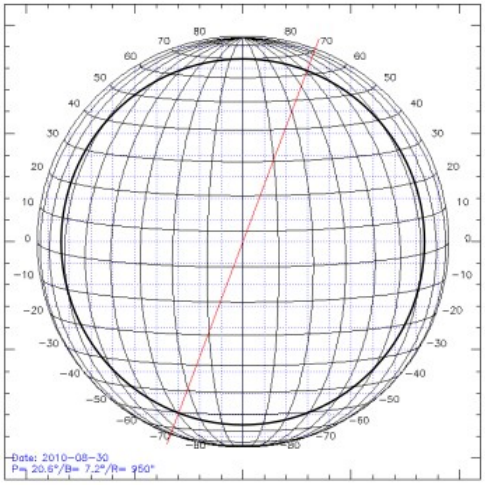

Fig. 6. Solar grid where the dark circle indicates the limit of the validity of the horizontal velocity measurement.

Spatial window = 2.5 Mm
Temporal window = 1 hour

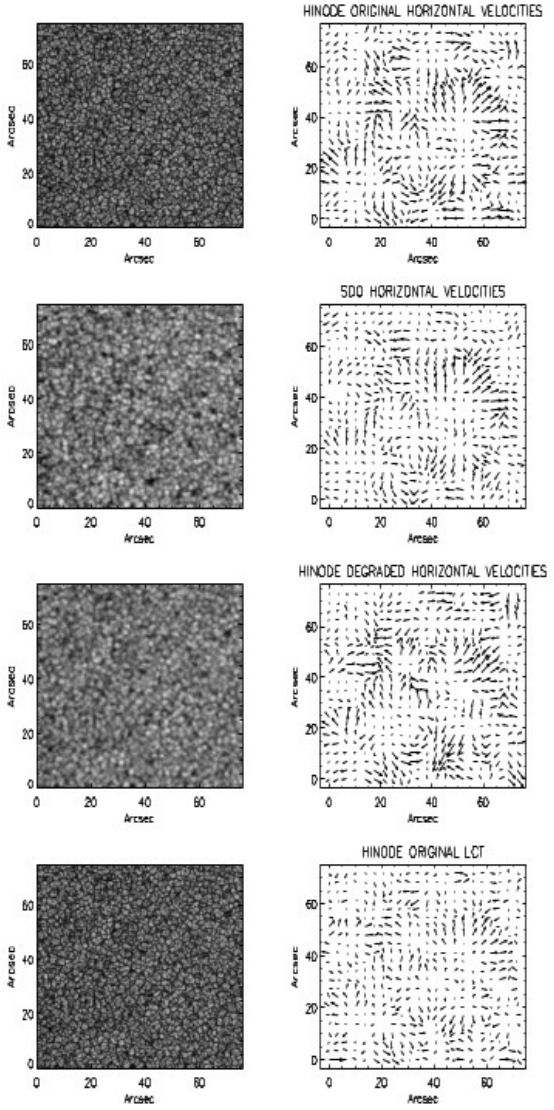

CST (Roudier 2012)
Full Sun

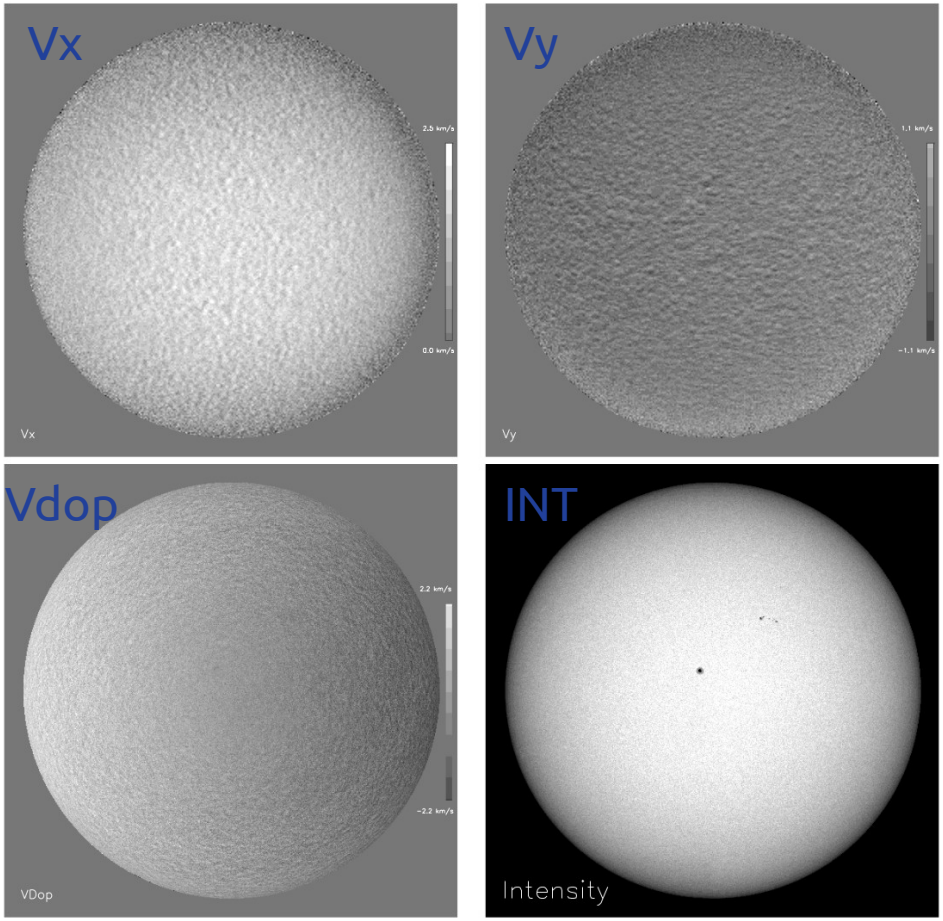

Fig. 11. v_x, v_y, $v_{\rm Dop}$ velocity maps for the three-hour sequence on August 30, 2010, and the intensity at the beginning of the sequence.

Spatial window = 2.5 Mm
Temporal window = 30 minutes

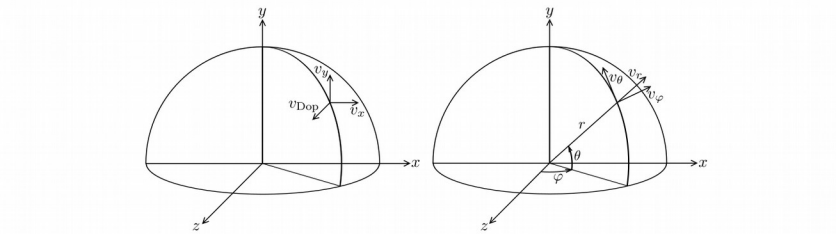

Fig. 10. Coordinate systems used throughout this paper: velocity components in the sky plane v_x and v_y and the line of sight velocity $v_{\rm Dop}$ (*left*); velocity components on the solar surface v_r, v_φ, v_θ (*right*).

CST (Roudier 2012)
Full Sun

V_r

Vφ

Vθ

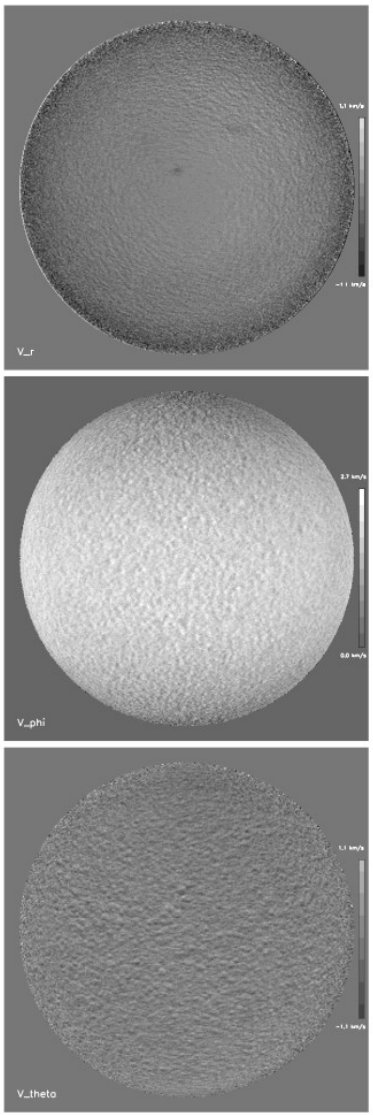

Fig. 12. $v_r(\theta,\varphi), v_\theta(\theta,\varphi), v_\theta(\theta,\varphi)$ for the three-hour sequence on August 30, 2010.

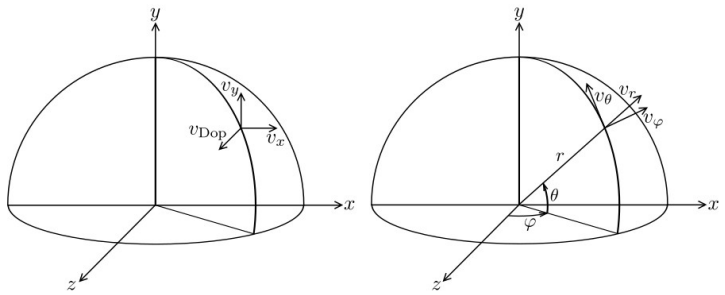

Fig. 10. Coordinate systems used throughout this paper: velocity components in the sky plane v_x and v_y and the line of sight velocity $v_{\rm Dop}$ (*left*); velocity components on the solar surface v_r, v_φ, v_θ (*right*).

θ=latitude
φ=longitude

$$
\begin{aligned}
v_r(\theta,\varphi) &= \cos\theta * \sin\varphi * v_x \\
&\quad + (\sin\theta * \cos B_0 - \cos\theta * \cos\varphi * \sin B_0) * v_y \\
&\quad + (\cos\theta * \cos\varphi * \cos B_0 + \sin\theta * \sin B_0) * v_{\rm Dop} \\
v_\theta(\theta,\varphi) &= -\sin\theta * \sin\varphi * v_x \\
&\quad + (\sin\theta * \cos\varphi * \sin B_0 + \cos\theta * \cos B_0) * v_y \\
&\quad + (\cos\theta * \sin B_0 - \sin\theta * \cos\varphi * \cos B_0) * v_{\rm Dop} \\
v_\varphi(\theta,\varphi) &= \cos\varphi * v_x \\
&\quad + \sin\varphi * \sin B_0 * v_y \\
&\quad - \sin\varphi * \cos B_0 * v_{\rm Dop}.
\end{aligned}
$$

B0= angle cf film

CST (Roudier 2012)
Solar differential rotation

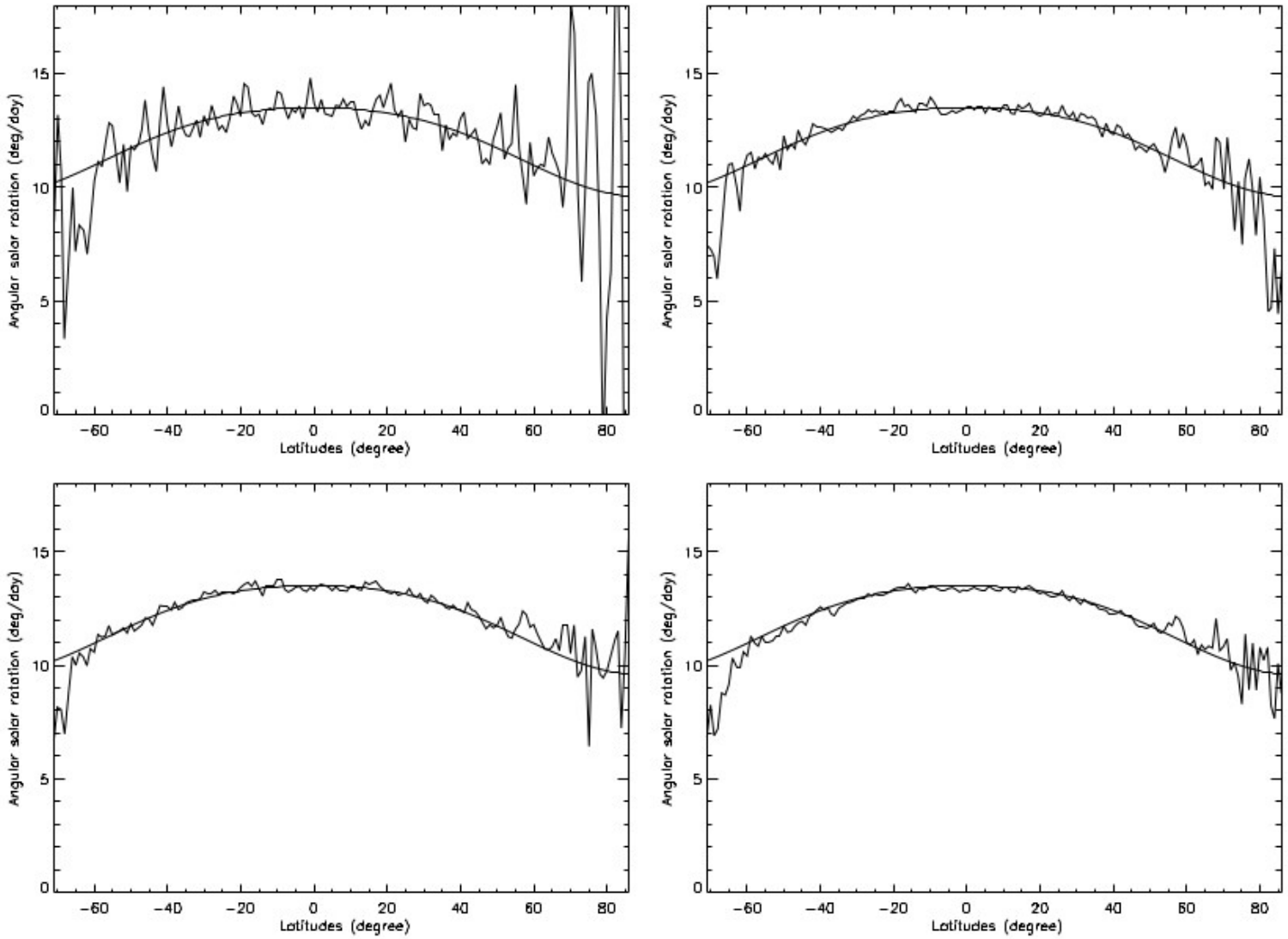

Fig. 13. Solar differential rotation on August 30, 2010, computed for the four different angles: 2° (*top left*), 10° (*top right*), 20° (*bottom left*), 40° (*bottom right*) either side of the central meridian.

CST (Full Sun data reduction)

HMI/SDO data

Prepare
Doppler files (586x586)
Intensiy files (4096x4096)

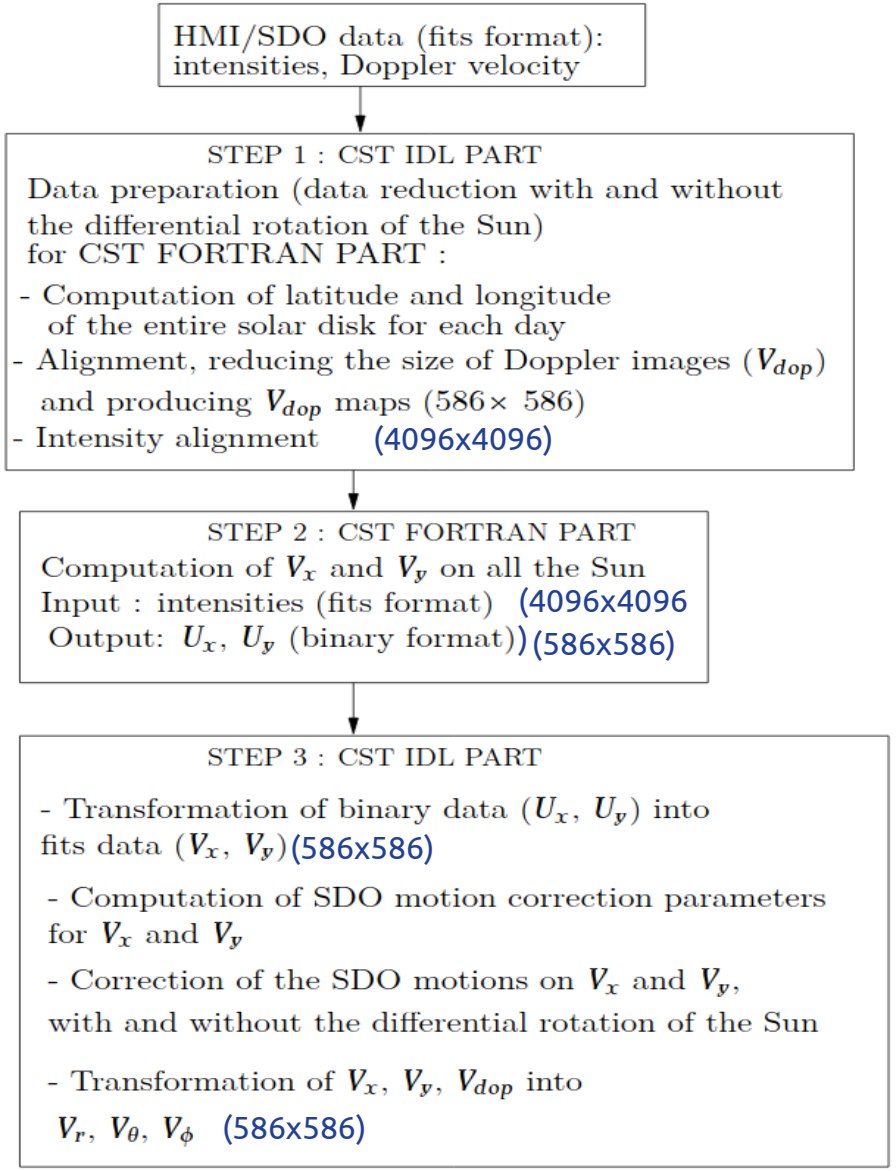

IDL

Fortran

IDL

Figure 1: Scheme of CST codes

CST (Roudier 2012)
Full Sun

Photospheric velocity field reconstruction

HMI Intensity and Doppler (4096 × 4096, JSOC) ===> to obtain 3 components of the photospheric velocity field (u x , u y , u z)

FOR DEROTATION : Measured on Doppler data or used a default

Default CST rotation profile adjusted from the raw Doppler data averaged over the 24 h of observations (quiet Sun):

Ω(λ) = 2.68 − 0.52 sin 2 (λ) − 0.29 sin 4 (λ) μrad s −1 , where λ is the latitude.

Nota :convention is that u Dop is taken as positive when the flow is away from the observer, so that the out-of-plane velocity towards the observer is $u_z \simeq -u_{\mathrm{Dop}}$

I) STEP I : CST IDL 30min SDO sequence (takes 1200 sec soit 20 mn)

.r reduction_doppler_intensity_all_days_apres_TP_7nov2019.pro

We used the default solar rotation

Doppler preparation

1) adjust solar position and diameter to the solar position and diameter of the first image (reference image) ; SDO orbital effects
2) correction of the SDO motions on Doppler
3) limbshift correction
4) mean of the corrected Doppler Doppler_with_rotation.dat ; idl file size (586,586,48)
5) Solar rotation determination =====> omega_doppler.dat
6) Derotation of the Doppler : we use either the measured rotation or the standard rotation Ω(λ) defined above.
===>Doppler_derot_raw ; files 586x 586 pixels
===>Doppler_derot_smooth ; files 586x 586 pixels
7) mean of the derotated files by 30min (40 frames) ===> Doppler_derot_30mn.dat

Préparation des Intensités

8) adjust solar position and diameter to the solar position and diameter of the first image (reference image) ; SDO orbital effects
9) Derotation of the intensity (input files for the step II fortran)

CST (Roudier 2012)
Full Sun

I) STEP I : CST IDL

Formulae of the correction

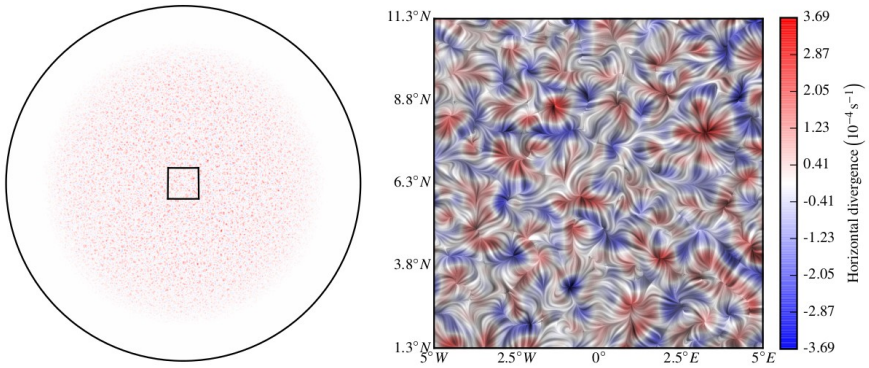

first substracted the rotational Doppler shift

$$u_{\mathrm{Dop}}^{\mathrm{rot}} = \Omega(\lambda)\, \sin\varphi\, \cos\lambda\, \cos B_0\, R_\odot, \tag{A.4}$$

where $\Omega(\lambda)$ is given in Eq. (A.1), and the Doppler shift associated with the satellite motion

$$u_{\mathrm{Dop}}^{\mathrm{sat}} = V_R \cos\sigma - V_W\,(x/D_\odot) - V_N\,(y/D_\odot), \tag{A.5}$$

where $\sigma = \arcsin\left(\sqrt{x^2+y^2}/D_\odot\right)$. The images were subsequently "derotated" in the same way as the white-light images and further corrected from a polynomial radial limbshift function adjusted from ring averages of two hours of data taken at different heliocentric angles from disc center ρ,

$$u_{\mathrm{Dop}}^{\mathrm{limb}} = \left(-0.35\,x + 0.2\,x^2 + 0.46\,x^3\right) \mathrm{km\,s^{-1}}, \tag{A.6}$$

where $x = 1 - \cos\rho$ and

$$\rho = \arcsin\sqrt{\sin^2\theta \sin^2\varphi + (\cos\theta\cos B_0 - \sin\theta\cos\varphi\sin B_0)^2}. \tag{A.7}$$

Since the 586^2 velocity-field maps derived from the CST have a 2.5 Mm spatial resolution, we then downsampled the 4096^2 Dopplergrams to 586^2, keeping only one point out of seven in each direction, and averaged over 30-min periods to obtain an effective sequence of maps of u_z, with the same spatial and temporal resolution as that of the (u_x, u_y) maps derived from CST.

CST (Roudier 2012)
Full Sun

I) STEP I : CST IDL

DEROTATION

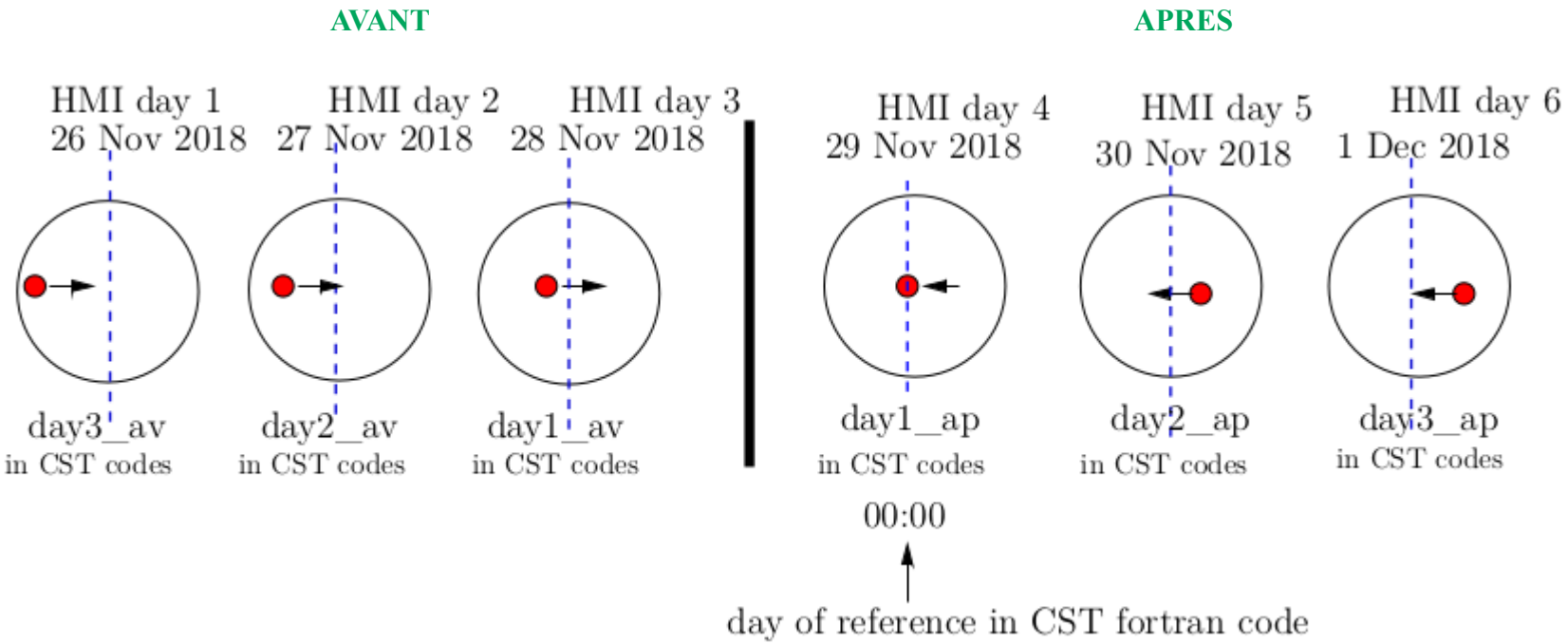

I) STEP II : CST Fortran (chez Thierry sous olympe CALMIP Toulouse)

param_seq_29nov2018_EOS_30mn

```
#nconv = 5
#nconv = 3
nconv = 1

option = vitesse # 1 options : segmentation, vitesse, trajectoires

#ip_start = 1 # numero de la plaque de demarrage
istep = 1      # delta entre numero de plaque
nb_series = 1   # Nombre de series independantes
ngmax0   = 900000 # Nombre max de granule par frame
ngmax    = 25000000 # Nombre max de granule au total
np       = 40 # Nombre de plaques              #pour la derniere de 24h
n_ech    = 40 # Frequence d'echantillonnage

n_life   = 60    # Duree de vie max des granules en nb de plaques
bin_sp   = 7    # bin spatial en pixels pour le champ de vitesse
v_thres  = 7.0   # Largest authorized velocity in km/s
t_thres  = 180.   # Minimum lifetime of a granule to be used in seconds
seuil_min= 0.01   # Min threshold for granule identification (in pix)

segmentation_type = strouss # Type of segmentation: strouss, CD, CD2, CD3

suffix = .fits                  # suffix des fichiers

prefix =/tmpdir/roudier/day1/day1_apres_int_derot_
input_file = param_seq_29nov2018_EOS_30mn

#for the 29 nov 2018    696000.km /972.877991  arcsec 715.403 km=1arcsec

arcsec = 715.403    # la valeur de la seconde d'arc en km
timestep =  45.      # la valeur du pas de temps en secondes.
pixel= 0.504008     # la taille du pixel en seconde d'arc

# Dimension/position de la sous-image (nx1:nx2,ny1:ny2)

#nx2=256
#ny2=256

verbose=1      # degre de detail des prints
```

dans param_seq_29nov2018_EOS_30mn

for the 29 nov 2018 696000. km / 972.877991 arcsec soit 715.403 km/arcsec

rayon du soleil =696000. km
rayon du soleil en arcsec = 972.877991
Dans le header fits, par example des fichiers Doppler :
RSUN_OBS=INDEX.RSUN_OBS ; R Sun in arcsec

pixel= 0.504008 provient de pix=INDEX.CDELT1

Additionnal informations

In **cst_labv7_FS_2017.f90**
mask to isolate the Sun (to avoid noise outside the Sun) can be modified.

R_sol=1873.	Mask radius in pixel
x_cent= 2054.47	X mask center
y_cent= 2048.21	Y maskcenter

I) STEP II : CST Fortran (chez Thierry sous olympe CALMIP Toulouse)

script_th2018_29nov2018_30mn_18coeurs_TEST.slurm

```
#!/bin/bash
#SBATCH -J script_art435
#SBATCH -N 1
#SBATCH -n 1
#SBATCH --threads-per-core=1
#SBATCH --cpus-per-task=36
#SBATCH --time=100:00:00

module purge
module load intel/18.2
#module load intel/11.1
module li
#make clean
#make
workdir=${SLURM_SUBMIT_DIR}/JOB_${SLURM_JOBID}
mkdir ${workdir}
cd ${workdir}

#lfs setstripe -c 1 .

cp $0 .
export OMP_NUM_THREADS=${SLURM_CPUS_PER_TASK}
MKL_NUM_THREADS=$OMP_NUM_THREADS

#cp ../cst_labv7_FS_2017 .
cp ../cst_labv7_FS_2017 .
cp ../param_seq_29nov2018_EOS_30mn .
mkdir results
cp ./param_seq_29nov2018_EOS_30mn param_2018_EOS_tempo

NINDEX=0            #indice de boucle  1ere heure
```

script_th2018_29nov2018_30mn_18coeurs_TEST.slurm (suite)

```
#while [ $NINDEX -le 47 ]       #on decide jusqu'a va la boucle
while [ $NINDEX -le 0 ]         #on decide jusqu'a va la boucle

do
      let NSTART=40*$NINDEX+1    #indice de depart
            Nfich=$(printf "%04d" $NINDEX)
            echo $Nfich
      echo "New execution: starting frame $NSTART"
      cp param_seq_29nov2018_EOS_30mn param_2018_EOS_tempo #on copie le fichier de
parametre de depart dans un temporaire
      echo "ip_start=$NSTART # numero de la plaque de demarrage">> param_2018_EOS_tempo
#on ajoute une ligne
sed -i 's#param_seq_29nov2018_EOS_30mn#param_2018_EOS_tempo#g' param_2018_EOS_tempo
srun -N 1 -n 1 -c $OMP_NUM_THREADS cst_labv7_FS_2017 < param_2018_EOS_tempo  >>
output_${SLURM_JOBID}.log

    #liste des fichiers a renommer
            echo ${workdir}
            mv ${workdir}/results/div1b ${workdir}/results/div_b_$Nfich
            mv ${workdir}/results/div1h ${workdir}/results/div_h_$Nfich
            mv ${workdir}/results/div1k ${workdir}/results/div_k_$Nfich
            mv ${workdir}/results/div1l ${workdir}/results/div_l_$Nfich
            mv ${workdir}/results/div1m ${workdir}/results/div_m_$Nfich
            mv ${workdir}/results/err1b ${workdir}/results/err_b_$Nfich
            mv ${workdir}/results/err1h ${workdir}/results/err_h_$Nfich
            mv ${workdir}/results/err1k ${workdir}/results/err_k_$Nfich
            mv ${workdir}/results/err1l ${workdir}/results/err_l_$Nfich
            mv ${workdir}/results/err1m ${workdir}/results/err_m_$Nfich
            mv ${workdir}/results/rot1b ${workdir}/results/rot_b_$Nfich
            mv ${workdir}/results/rot1h ${workdir}/results/rot_h_$Nfich
            mv ${workdir}/results/rot1k ${workdir}/results/rot_k_$Nfich
            mv ${workdir}/results/rot1l ${workdir}/results/rot_l_$Nfich
            mv ${workdir}/results/rot1m ${workdir}/results/rot_m_$Nfich
            mv ${workdir}/results/ux1b ${workdir}/results/ux_b_$Nfich
            mv ${workdir}/results/ux1h ${workdir}/results/ux_h_$Nfich
            mv ${workdir}/results/ux1k ${workdir}/results/ux_k_$Nfich
            mv ${workdir}/results/ux1l ${workdir}/results/ux_l_$Nfich
            mv ${workdir}/results/ux1m ${workdir}/results/ux_m_$Nfich
            mv ${workdir}/results/uy1b ${workdir}/results/uy_b_$Nfich
            mv ${workdir}/results/uy1h ${workdir}/results/uy_h_$Nfich
            mv ${workdir}/results/uy1k ${workdir}/results/uy_k_$Nfich
            mv ${workdir}/results/uy1l ${workdir}/results/uy_l_$Nfich
            mv ${workdir}/results/uy1m ${workdir}/results/uy_m_$Nfich
            mv ${workdir}/results/nb_gran ${workdir}/results/nb_gran_$Nfich
            mv ${workdir}/results/param_2018_EOS_tempo
${workdir}/results/param_2018_EOS_tempo_$Nfich
            mv ${workdir}/results/traject1_11 ${workdir}/results/traject_11_$Nfich
```

I) STEP III : CST IDL

ux,uy (binaire) ===> fits Vx et Vy

.r transform_uxuy_vxvy_all_dates_step_30min_fev2020.pro

Correction des mvt de SDO sur les Vx et Vy

.r correct_mvtSDO_sur_Vx_et_Vy_precis_all_dates_apres_fev2020.pro

$$u_x^{\mathrm{sat}}(x,y,t) = -V_W(t)/D_\odot \sqrt{R_\odot^2 - (x^2+y^2)}, \qquad \text{(A.2)}$$

$$u_y^{\mathrm{sat}}(x,y,t) = -V_N(t)/D_\odot \sqrt{R_\odot^2 - (x^2+y^2)}, \qquad \text{(A.3)}$$

Transformation des Vx,Vy, Vdop en Vr, Vthe,Vphi (sphérique)

.r transfor_Vx_Vy_Vdop_vthe_vphi_vr_all_dates_4juillet2019_fev2020.pro

Nota : - 24 cores is recommanded above noise increases (a little)
- **limitation to 60° latitude and longitude.**
- **for 6 days the zero of the Doppler are not centered (take care)**
- **and also the derotation beyond the 4 days is limited because the Doppler component on the limb represents the horizontal component therefore a Vx and or Vy when we derote. This component is normally measured by the CST(!).**

CST (Roudier 2012)
Full Sun

I) STEP I : CST IDL

DEROTATION

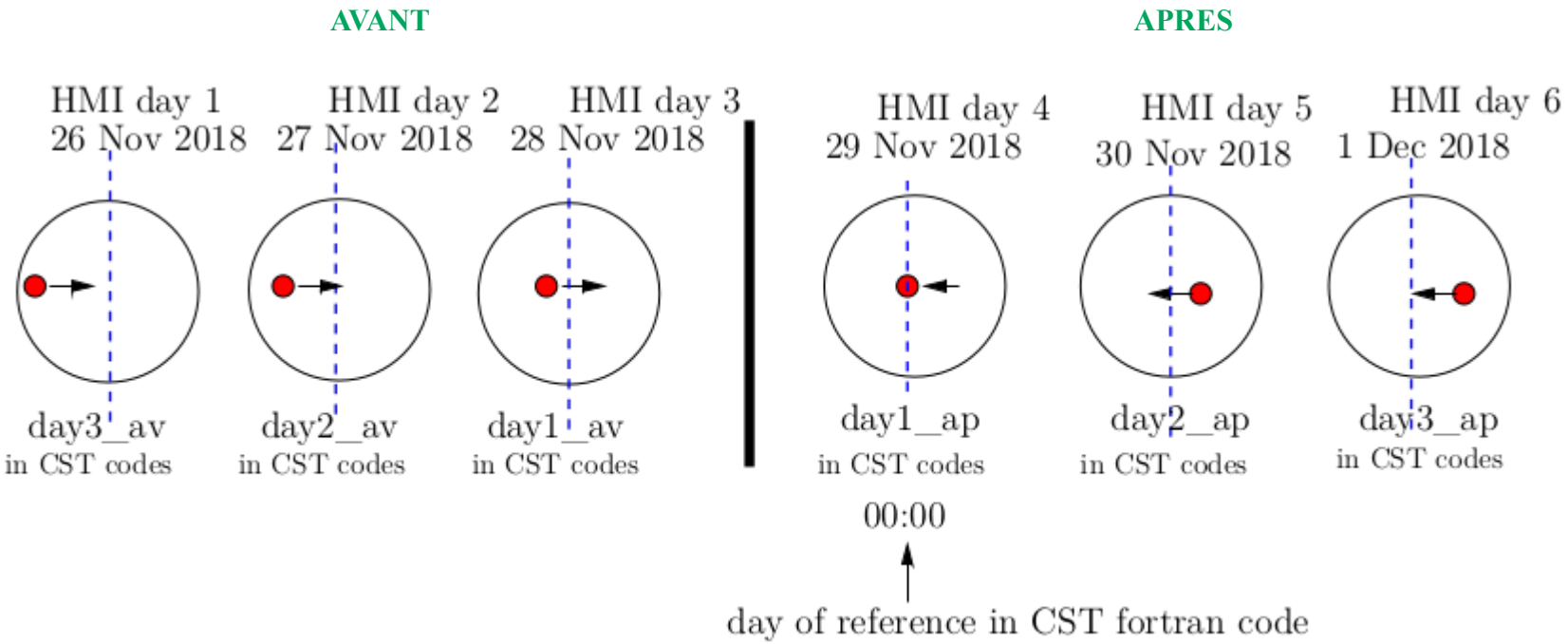

1 to 3 days data reduction

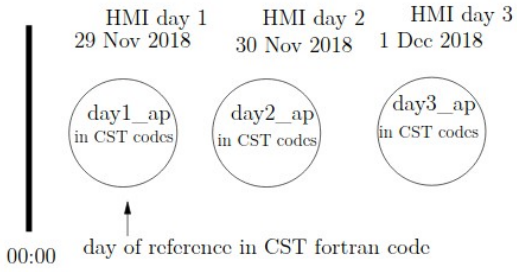

Figure 5: CST run for 3 observation days. The 1st day (November 29, 2018) is the reference day.

Derotation avant
Derotation apres

Different direction of rotation in « avant » and « apres »

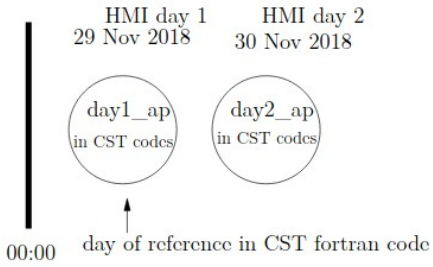

Figure 6: CST run for 2 observation days. The 1st day (November 29, 2018) is the reference day.

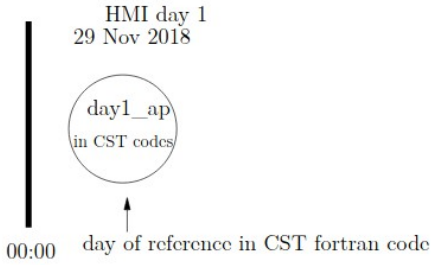

Figure 7: CST run for 1 observation day. The observation day (November 29, 2018) is the reference day.

4 to 6 days data reduction

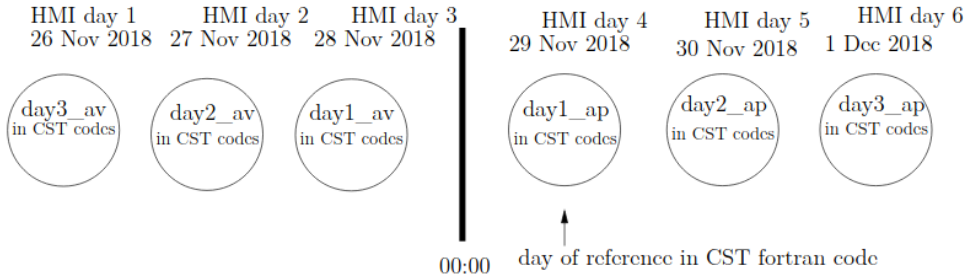

Figure 2: CST run for 6 observation days. The 4th day (November 29, 2018) is the reference day.

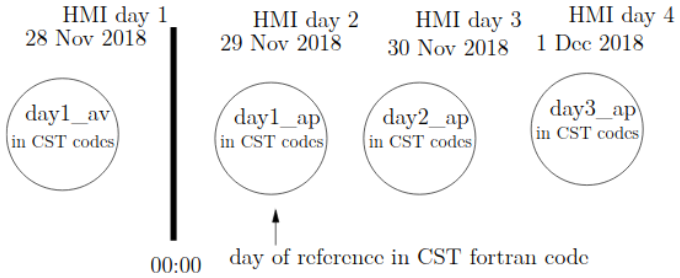

Figure 3: CST run for 4 observation days. The 2nd day (November 29, 2018) is the reference day.

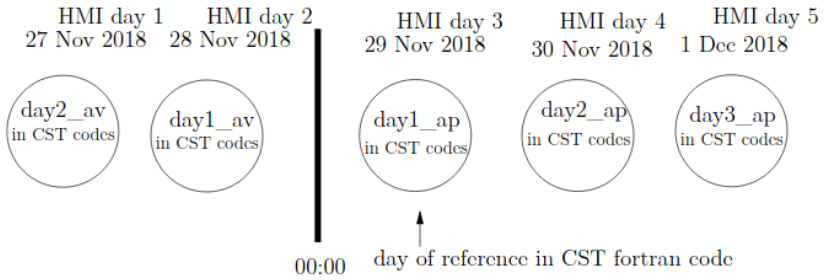

Figure 4: CST run for 5 observation days. The 3rd day (November 29, 2018) is the reference day.

CST DATA REDUCTION 6 days

INPUT

HMI (Int et Dop) data in directories

day	
1	day1_ap
2	day2_ap
3	day3_ap
-1	day1_av
-2	day2_av
-3	day3_av

STEP I : IDL (20 min for each 30min sequence)

Select the number of day, with or without solar rotation

reduction_doppler_intensity_all_days_apres.pro
reduction_doppler_intensity_all_days_avant.pro

STEP II : FORTRAN (2 days for 24h sequence)

(All the scripts can be run at the same time)

param_seq_day1_apres_EOS_30mn
script_th2018_day1_apres_30mn_18coeurs.slurm

param_seq_day2_apres_EOS_30mn
script_th2018_day2_apres_30mn_18coeurs.slurm

param_seq_day3_apres_EOS_30mn
script_th2018_day3_apres_30mn_18coeurs.slurm

param_seq_day1_avant_EOS_30mn
script_th2018_day1_avant_30mn_18coeurs.slurm

param_seq_day2_avant_EOS_30mn
script_th2018_day2_30mn_18coeurs.slurm

param_seq_day3_avant_EOS_30mn
script_th2018_day3_30mn_18coeurs.slurm

STEP III : IDL (a few minutes)

Here for high resolution « h » files

Select the number of day, with or without solar rotation

rotation.step3_CST_IDL_apres.pro (old version)
rotation.step3_CST_IDL_avant.pro (old version)

rotation.step3_CST_IDL.pro (new version)

OUTPUT

First create the directories

day	
1	treated_day1_ap
2	treated_day2_ap
3	treated_day3_ap
-1	treated_day1_av
-2	treated_day2_av
-3	treated_day3_av

OUTPUT

To visualize the last segmented image image_cont of each sequence (CST) use :

visu_gran_seg_FS.pro

ABSTRACT

CoherentStructureTracking (CST) algorithm (Roudier et al.(2012);Švanda et al.(2013);Roudier et al.(2013);Rincon et al.(2017);Roudier et al. (2018)) is a set of codes written in IDL and Fortran 90, computing the horizontal velocity field on the Sun surface by using solar granules as tracers

CST codes take as input HMI/SDO intensity images (hmi.Ic_45s),with a time step of 45s.

Each record includes a list of keywords and one image of the Sun(2D, 4096x4096) in FITS format.

We use also the HMI/SDO Dopplergrams (hmi.V_45s),to derive spherical velocities on the Sun surface.

The Vx andVy (in km/s) are computed ata cadence of 30 min with a spatial window of 7 pixels, equivalent to 3.5 arcsec, around 2.5 Megameters (Mm) (Rieutord et al.,2001).

HMI/SDO data have the North at the bottom and East on the right of the image; the images are rotated in order to have the North on top and East on the left.

To read and treat HMI/SDO data, we use SSWIDL and ifort compiler. The Fortran part is parallelized with OpenMP

Ce que l'on peut améliorer : deconvoluer les images de SDO , fenetre temporelle de 15 min. et spatiale de 1.25 Mm.

OPEN QUESTIONS: code in evolution (python version), automating
deconvoluted data of HMI/SDO can be used ⇒ 15min, 1.25 Mm windows

Examples avec et sans rotation solaire (Full Sun)

CST results (movies) , solar rotation, filament destabilization solar Coronna, dynamic of the photosphere

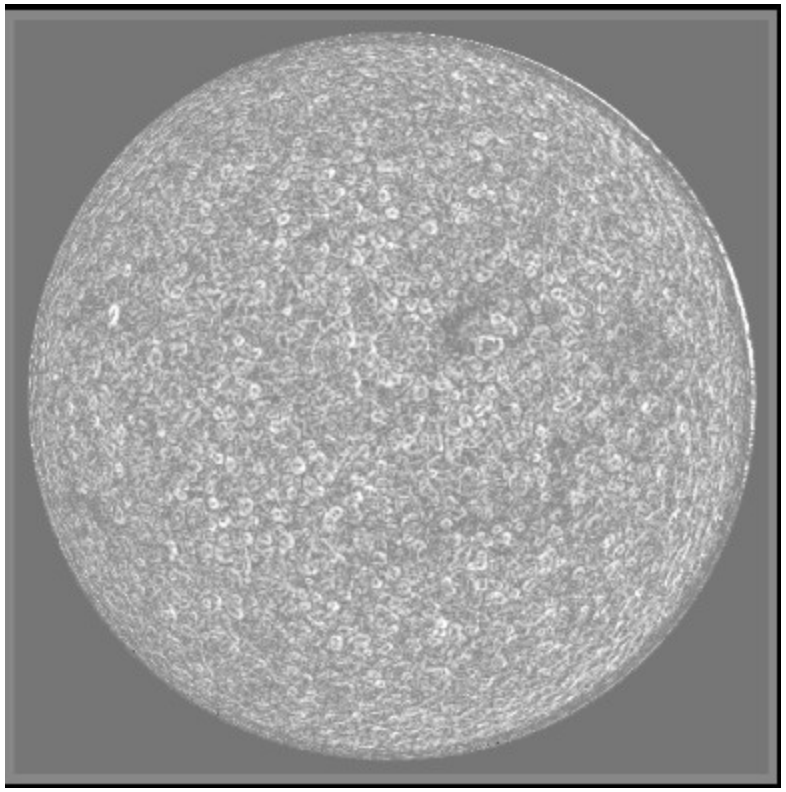

Next WORKSHOP 2021

Movies

6days_fen1h_pas30min.mp4
div6days.mp4
div-V-6days.mp4
div-cst-sdo.mp4
module.mp4

2018_10_31_00_00_53_2018_11_01_00_37_53_AIA_193-hq.mp4
B+V_31oct2018.mp4
B+V+UV_31octobre2018.mp4
V-B-UV193.mp4

movie5.mp4

SDO_deconv.mp4
SDO_deconv_align.mp4
SDO_deconv_align_filt_2kms.mp4

SDO_fam_vh.mp4
balancement.wmv